JOURNAL OF SPACECRAFT AND ROCKETS
Vol. 41, No. 6, November–December 2004

# Linear and Pendular Acceleration Effects in Fluid Dynamic Experiments Under Low Gravity

R. Savino,* D. Paterna,† and F. Nota‡
*University of Naples "Federico II," 80125 Naples, Italy*

**To study the influence of residual acceleration on fluid physics experiments in microgravity environments, the different driving forces in the vorticity equation (leading to convective motion in a fluid cell) are considered. Steady and linear time-dependent accelerations generate convection in an otherwise quiescent fluid only in the presence of density gradients. Pendular acceleration may induce convective motion even in the absence of a density gradient induced by temperature and/or species concentration differences. Numerical simulations are carried out for different study cases, in the presence of low-frequency and high-frequency oscillations, based on realistic values of the accelerations onboard space platforms. The numerical results are compared with experimental results, obtained in microgravity and ground laboratories.**

## Nomenclature

| | | |
|---|---|---|
| $c$ | = | species mass fraction |
| $D$ | = | diffusion coefficient, m$^2$/s |
| $d$ | = | fluid particle distance from the center of mass, m |
| $f$ | = | frequency, Hz |
| $g$ | = | gravity acceleration, m/s$^2$ |
| $k$ | = | segregation coefficient |
| $\boldsymbol{k}$ | = | unit vector |
| $L$ | = | cell length, m |
| $n$ | = | direction normal to the cell wall |
| $Pe$ | = | Peclet number |
| $p$ | = | pressure, Pa |
| $R$ | = | radius, m |
| $\boldsymbol{r}$ | = | position vector, m |
| $T$ | = | temperature, K |
| $t$ | = | time, s |
| $u, v$ | = | velocity components along the $x$, $y$ axes, m/s |
| $\boldsymbol{V}$ | = | velocity vector, m/s |
| $x, y, z$ | = | Cartesian coordinates, m |
| $\alpha$ | = | angular displacement, rad |
| $\dot{\alpha}, \Omega$ | = | angular velocity, rad/s |
| $\ddot{\alpha}, \dot{\Omega}$ | = | angular acceleration, rad/s$^2$ |
| $\beta_c$ | = | solutal expansion coefficient |
| $\beta_T$ | = | themal expansion coefficient, 1/K |
| $\boldsymbol{\Theta}$ | = | unit vector |
| $\nu$ | = | kinematic viscosity, m$^2$/s |
| $\rho$ | = | density, kg/m$^3$ |
| $\Psi$ | = | gravitational potential, m$^2$/s$^2$ |
| $\psi$ | = | stream function, m$^2$/s |
| $\boldsymbol{\omega}$ | = | vorticity, 1/s |

*Subscripts*

| | | |
|---|---|---|
| $a$ | = | external forces |
| $c$ | = | center of mass |
| $d$ | = | fluid particle displacement |
| $i$ | = | $i$th species in the fluid mixture or $i$th term in the Fourier series |
| $k$ | = | $k$th term in the Fourier series |
| $R$ | = | cell distance from the rotation axis |
| 0 | = | reference conditions |

Received 13 February 2003; revision received 10 October 2003; accepted for publication 24 October 2003. 

*Associate Professor of Fluid Dynamics, Department of Space Science and Engineering "Luigi G. Napolitano," P. le Tecchio, 80.

†Research Scientist, Department of Space Science and Engineering "Luigi G. Napolitano," P. le Tecchio, 80.

‡Ph.D. Student, Department of Space Science and Engineering "Luigi G. Napolitano," P. le Tecchio, 80.

## Introduction

MOST of the planned experimentation on orbiting spacecraft is motivated by the attempt to establish processes in which scalar extensive quantities (species and/or energy) can be transported by diffusion only. However, different acceleration disturbances are present in the microgravity environment of space platforms such as the International Space Station. These accelerations may induce convective velocities and, therefore, thermofluiddynamic distortions in otherwise quiescent liquid phases. To date, nearly all of the works that address the influence of the microgravity environment on fluid physics experiments are based on numerical modeling and scaling analysis.[1–9] Generally they are focused on the effects of quasi-steady or periodic linear accelerations in fluid systems with density gradients, based on predictions of the expected amplitudes and frequencies of the accelerations. A review of the subject is presented by Savino and Monti.[10]

A careful analysis of the microgravity environment onboard orbiting platforms[11–13] indicates that not only linear accelerations but also pendular motions can be present at the payload locations, due to rigid-body oscillations around the center of mass of the station and to elastic deformations of the structure. Therefore, the study of the effects of pendular oscillations (at different frequencies) is very important.

In this paper, the Navier–Stokes equations are analyzed to identify the terms in the momentum and vorticity equations that generate convective motions in a fluid cell. Most of the results will be presented for relatively small temperature and/or species concentration gradients, so that the fluid density can be considered almost uniform and the distortions of the temperature and/or concentration field, induced by pendular accelerations, can be analyzed. Some problems have been identified to study the effects of oscillating (linear and/or pendular) accelerations. In particular, experimental results obtained onboard the Russian capsule Foton,[13] numerically correlated with the present model, show the importance of pendular motions. A numerical analysis is carried out for the selected study cases, for the quasi-steady and periodic accelerations. The recent NASA measurements[14–16] and/or predictions for the International Space Stations are considered.

The paper is setup as follows. The next section is dedicated to the analysis of the driving forces (in the momentum and vorticity equations) associated with the different accelerations disturbances (quasi

steady, time dependent, linear, pendular). The section after that deals with the numerical models used to solve the governing equations for the different problems considered in this paper. Following that discussion, the experimental results and the numerical simulations of a fluid physics experiment performed in microgravity conditions onboard the Russian space capsule Foton are discussed. The numerical simulations related to three different possible experiments of interest for the International Space Station (ISS) (nonisothermal cell filled with a homogeneous liquid, diffusion experiment, Bridgman crystal growth) are discussed subsequently. Laboratory experiments and numerical simulations for the analysis of the streaming flow induced by pendular oscillations in an isothermal fluid cell are then presented.

## Effects of Acceleration Disturbances on Orbiting Spacecraft

Convection in an otherwise quiescent fluid (no motion imposed at the boundaries) is due only to the presence of a nonuniform body force $\rho g$. Indeed, the continuity and momentum equations, under the Boussinesq approximation, are

$$\nabla \cdot \boldsymbol{V} = 0 \tag{1}$$

$$\frac{\mathrm{D}\boldsymbol{V}}{\mathrm{D}t} = \frac{\partial \boldsymbol{V}}{\partial t} + \boldsymbol{V} \cdot \nabla \boldsymbol{V} = -\frac{\nabla p}{\rho_0} + \nu \nabla^2 \boldsymbol{V} + \frac{\rho}{\rho_0}\boldsymbol{g} \tag{2}$$

Using well-known vectorial identities, and taking the curl of Eq. (2) to derive the vorticity equation, one obtains

$$\frac{\mathrm{D}\boldsymbol{\omega}}{\mathrm{D}t} - \boldsymbol{\omega} \cdot \nabla \boldsymbol{V} - \nu \nabla^2 \boldsymbol{\omega} = \frac{\rho}{\rho_0} \nabla \times \boldsymbol{g} + \nabla\left(\frac{\rho}{\rho_0}\right) \times \boldsymbol{g} \tag{3}$$

One can identify the production term for $\boldsymbol{\omega}$ (driving force) in the two terms on the right-hand side of Eq. (3).

For a liquid enclosed in an impermeable cell, quiescent conditions, $\boldsymbol{V} \equiv \boldsymbol{0}$ and $\boldsymbol{\omega} \equiv \boldsymbol{0}$, can be established if the driving terms are zero; this is true for a conservative body force $\boldsymbol{g}$ so that $\boldsymbol{g} = \nabla \Psi$ and if the density gradient ($\nabla \rho$ is either zero or parallel to $\boldsymbol{g}$. In other cases, the body forces generate convection (because of non uniformity, within the fluid cell, either of $\boldsymbol{g}$ and/or of $\rho$). The vector $\boldsymbol{g}$ that appears in Eq. (3) is typically formed as follows: 1) steady (or quasi-steady) residual acceleration due to a) position of the cell with respect to the vehicle center of mass, b) steady rotation around the center of mass, typical of space shuttle flights, c) external forces (aerodynamic drag, solar pressure), and d) possible centrifugal forces due to steady rotations of the fluid cell around an axis and 2) unsteady $g$-jitter due to different causes that can be grouped into two categories, a) periodic acceleration with zero time average (crew activity, disturbances induced by on board machinery) and b) pulselike disturbances due to single events, for example, docking, venting, boost to higher orbits, meteorite impacts.

In what follows we will assume that forces 1c do not induce angular accelerations but only linear accelerations; furthermore, we will not consider accelerations 2b because the time schedule for the microgravity experimentation does not foresee these events.

### Steady Accelerations

The model assumed is a platform that rotates around its center of mass with a constant angular velocity $\Omega_c$ and the center of mass follows a circular orbit of radius $R_c$ at which the gravity acceleration $g_c$ is equal and opposite to the centrifugal acceleration, $\Omega_c^2 R_c = g_c$. The space vehicle rotates around its $y$ axis to keep its $z$ axis oriented to nadir and its flight direction along the $x$ axis; $x$, $y$, and $z$ axes form the orthogonal coordinate system fixed to the platform with the origin in its center of mass (Fig. 1).

According to the coordinate system definition, the (residual) gravity vector $g_d$ due to a displacement ($d = \sqrt{x^2 + y^2 + z^2}$) of the fluid particle from the c.m. is

$$\boldsymbol{g}_d = (g_c/R_c)(-y\boldsymbol{j} + 3z\boldsymbol{k}) \tag{4}$$

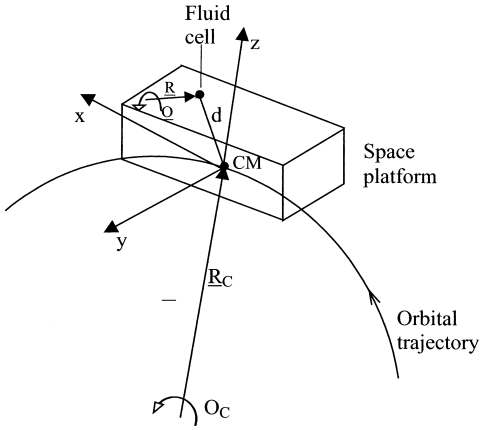


**Fig. 1 Coordinate system.**

which can be expressed in terms of a gravity gradient potential

$$\Psi_d = (g_c/2R_c)(3z^2 - y^2) \tag{5}$$

so that $\boldsymbol{g}_d = \nabla \Psi_d$.

Similarly, any constant linear acceleration due to forces acting on the outside of the vehicle (aerodynamic drag, solar pressure) that does not induce angular motions around the c.m. can be expressed as a function of a potential

$$\boldsymbol{g}_a = \nabla \Psi_a \tag{6}$$

When the cell rotates with a constant angular velocity vector $\boldsymbol{\Omega}$ around a rotation axis, then a nonuniform centrifugal body force in the fluid is generated that depends on the distance $\boldsymbol{R}$ of the cell point from the rotation axis. ($\boldsymbol{R}$ is orthogonal to $\boldsymbol{\Omega}$.) In this case, one can define a potential

$$\Psi_R = \Omega^2 R^2/2 \tag{7}$$

so that $\boldsymbol{g}_R = \nabla \Psi_R$.

To identify the forces that are responsible for the generation of convective flows starting from a quiescent ($\boldsymbol{V} = \boldsymbol{0}$) medium, we omit the Coriolis deviating force ($2\boldsymbol{V} \times \boldsymbol{\Omega}$) that exists only when there is already a convective motion inside the cell.

In conclusion, one may say that the first body force term ($\rho/\rho_0 \nabla \times \boldsymbol{g}$) is identically zero for the steady contributions,

$$\boldsymbol{g} = \nabla \Psi_d + \nabla \Psi_a + \nabla \Psi_R \tag{8}$$

### Time-Dependent Accelerations

Time-dependent terms can be subdivided into two categories: linear and pendular oscillations characterized by different amplitude time profiles. Typically these two categories can conveniently be expanded into two Fourier series:

$$\boldsymbol{g}_j(\boldsymbol{r}, t) = \sum_i \boldsymbol{g}_i \sin(2\pi f_i t) + \sum_k \boldsymbol{g}_k(\boldsymbol{r}, t) \tag{9}$$

The first expansion refers to linear accelerations, $\boldsymbol{g}_i = \nabla \Psi_i =$ const. The second expansion refers to pendular motions around different rotation axes and at different frequencies $f_k$, so that the acceleration is not constant within the fluid cell.

Let us consider the pendular motions first: If $\boldsymbol{r}_k$ is the position vector of the field point with respect to the axis around which the cell is rotating with a time-dependent angular velocity $\boldsymbol{\Omega}_k$, then the accelerations that the fluid particle experiences is

$$\boldsymbol{g}_k(\boldsymbol{r}, t) = \Omega_k^2 \boldsymbol{r}_k + \dot{\Omega}_k r_k \boldsymbol{\Theta}_k + 2\boldsymbol{V} \wedge \boldsymbol{\Omega}_k \tag{10}$$

that is, the centrifugal, the tangential, and the Coriolis accelerations. ($\boldsymbol{\Theta}_k$ is the unit vector along the tangent, orthogonal to $\boldsymbol{\Omega}_k$ and $\boldsymbol{r}_k$.)

To find the expression of $\boldsymbol{g}_k(\boldsymbol{r}, t)$ let us assume that the fluid cell follows a pendular motion around an axis. Let us denote the angular displacement by the angle $\alpha_k(t)$ given by

$$\alpha_k(t) = \alpha_{0k} \sin(2\pi f_k t) \tag{11}$$

The angular velocity and angular accelerations then are

$$\Omega_k(t) = \dot{\alpha}_k(t) = \alpha_{0k}(2\pi f_k)\cos(2\pi f_k t) \tag{12}$$

$$\dot{\Omega}_k(t) = \ddot{\alpha}_k(t) = -\alpha_{0k}(2\pi f_k)^2 \sin(2\pi f_k t) \tag{13}$$

consequently,

$$\boldsymbol{g}_k(\boldsymbol{r}, t) = \Omega_{0k}^2 \cos^2(2\pi f_k t)\boldsymbol{r}_k + \dot{\Omega}_{0k} \sin(2\pi f_k t) r_k \boldsymbol{\Theta}_k + 2\boldsymbol{V} \times \boldsymbol{\Omega}_{0k} \cos(2\pi f_k t) \tag{14}$$

where $\Omega_{0k} = \alpha_{0k}(2\pi f_k)$ and $\dot{\Omega}_{0k} = \alpha_{0k}(2\pi f_k)^2$.

In presence of more than one pendular oscillation with amplitude $\alpha_{0k}$ and frequency $f_k$, the overall $g$-jitter will include the summation over all of the pendular oscillations.

With reference to Eq. (14), the $g$-jitter terms whose curls are zero are the linear acceleration term and the centrifugal forces, which can be expressed in terms of the following potentials:

$$\Psi_i = g_i x_i, \qquad \Psi_{\Omega k} = \left(\Omega_k^2 r_k^2 / 2\right)\cos^2(2\pi f_k t) \tag{15}$$

where $x_i$ is the direction of the sinusoidal linear $g$-jitter ($\boldsymbol{\nabla}\Psi_i = \boldsymbol{g}_i$).

The terms with a nonzero curl are the tangential acceleration term,

$$\boldsymbol{\nabla} \times [\dot{\Omega}_{0k} \sin(2\pi f_k t) r_k \boldsymbol{\Theta}_k] = 2\dot{\Omega}_{0k} \sin(2\pi f_k t)\boldsymbol{k} \tag{16}$$

where $\boldsymbol{k} = \boldsymbol{r}_k / r_k \times \Theta_k$, and the Coriolis term,

$$\boldsymbol{\nabla} \times (\boldsymbol{V} \times \boldsymbol{\Omega}_{0k} \cos(2\pi f_k t)) \tag{17}$$

The terms that generate convective motion in a constant density and an otherwise quiescent fluid medium are

$$\frac{\rho}{\rho_0}\boldsymbol{\nabla} \times \boldsymbol{g} = 2\rho/\rho_0 \sum_k \alpha_{0k}(2\pi f_k)^2 \sin(2\pi f_k t)\boldsymbol{k} \tag{18}$$

due to a pendular motion of amplitude $\alpha_{0k}$ along the $\boldsymbol{k}$ axis.

In conclusion, in an isodense fluid, $\boldsymbol{\nabla}\rho \equiv 0$, only the pendular $g$-jitter terms (tangential accelerations) are able to produce momentum and vorticity.

## Numerical Model

The equations have been numerically solved using both a finite difference and a finite volume approach.[17] The three-dimensional computations are obtained with a finite volume technique, which solves the time-dependent Navier–Stokes equations (1) and (2) on a staggered grid in the primitive variable formulation of Monti and Savino.[7]

The two-dimensional results are obtained solving the equations on a col-located grid arrangement in the vorticity–stream function formulation. In particular, Eq. (3) has been discretized together with the Poisson equation for the stream function $\psi$:

$$\nabla^2\psi = -\omega \tag{19}$$

First-order forward finite differences have been used to discretize the time derivatives, whereas the convective terms have been computed numerically with a second-order upwind method; central differences have been used for the diffusive terms. The Poisson equation for the streamfunction has been solved with a successive overrelaxation method. No-slip conditions have been assigned on the cell walls, $u = \psi_y = 0$ and $v = -\psi_x = 0$.

Similarly, the transport equations have been solved with a finite difference method, using a first-order forward scheme for the time derivative, a second-order upwind scheme for the convective flux, and a second-order accurate central scheme for the diffusive term. The computations have been carried out in two- or three-dimensional domains (see following sections) using a uniform grid. Grid convergence is achieved in almost all of the computations because further grid refinement does not produce sensitive differences (less than 1%) in the results.

## Foton Capsule Case

Foton is a free-flying Russian retrievable capsule capable of accommodating experiment facilities and staying in low Earth orbit for about two weeks. The microgravity characteristics of the capsule were analyzed and documented after the Foton 11 and Foton 12 campaigns. In addition to a Russian and a French accelerometer, the payload was equipped with the quasi-steady acceleration measurement system (QSAM), a German development successfully tested on the Spacelab International Microgravity Laboratory IML-2 and Microgravity Science Laboratory MSL-1 missions. QSAM was also equipped with a tri-axial gyroscope that provides the angular accelerations of the spacecraft.[13]

The data obtained from Foton 11 and Foton 12 have demonstrated that, during almost the whole flight (with the exception of the insertion of capsule into orbit and of the deorbiting phase), the spacecraft was flown in free drift without any active control for the attitude.[13] The capsule assumes a stable gravity gradient orientation with a complex motion, characterized by a slow rotation around its $x$-symmetry axis (spin with an angular speed of the order of magnitude of 1 deg/s) and a precession of the $x$ axis along the local vertical with an angular velocity into the plane perpendicular to the $x$ axis of the order of 0.2 deg/s. Therefore, the microgravity environment at the payload location is characterized as follows: First, there is a quasi-steady acceleration (residual $\boldsymbol{g}$) caused by the slow rotation of the spacecraft around $x$ (spin) that causes, at the experiment location, a centrifugal force (of the order of 10 $\mu$g); second, there are pendular accelerations (along $y$, and $z$) of the order of 0.1 $\mu$g at the cell location and with the same period of the angular accelerations (order of 9 min).

The largest European payload was flown recently on Foton 12. One of the experiments was dedicated to thermal radiation aspects on migrating particles.[18] The aim of the experiment was the measurement of thermal radiation forces on tracers particles distributed in a liquid cell in presence of a temperature gradient.

A parallelepiped cell ($5 \times 5 \times 2$ cm$^3$) was filled with a solution of water and ethylene glycol (50% in concentration). A temperature gradient was established between two metallic opposite walls, to evaluate the tracers motion induced by thermal radiation forces (in the direction of the temperature gradient). Unfortunately, sometimes air bubbles were injected with the tracers. The drift motion of these bubble was always in the same direction, showing the presence of a quasi-steady residual $\boldsymbol{g}$. The order of magnitude of this acceleration and its direction can be evaluated looking at the position of the experimental cell in the Foton capsule (Fig. 2). As explained before, in addition to a pendular motion around the $y$ and $z$ axes, a rotation around the symmetry axis of the spacecraft was present, with an angular velocity of the order of 0.01–0.02 rad/s. Because of the distance of the cell from the symmetry axis [50 cm along $y$ and 9 cm along $z$ (Fig. 2)] the cell was subject to a centrifugal force (of the order of 10 $\mu$g). The direction and the value of the residual-$\boldsymbol{g}$

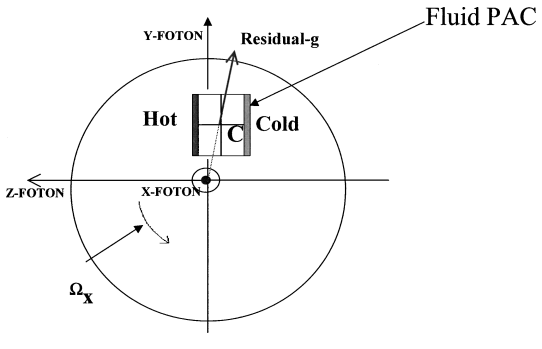


**Fig. 2 Position of the experimental cell in the Foton capsule.**

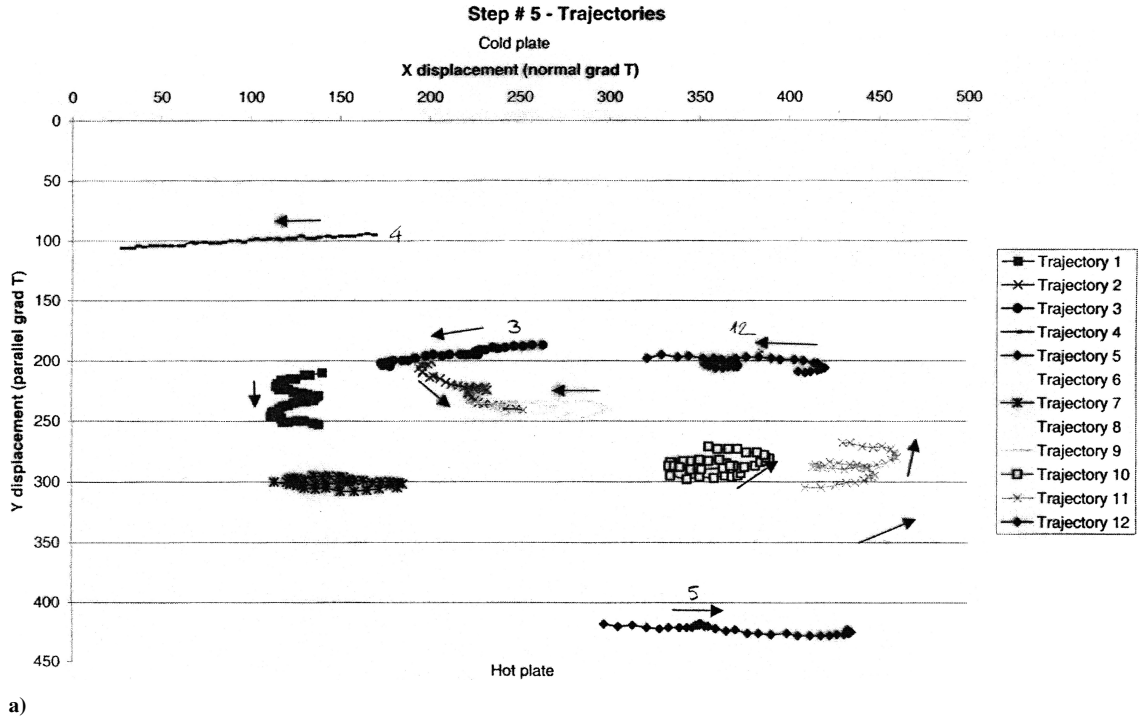


a)

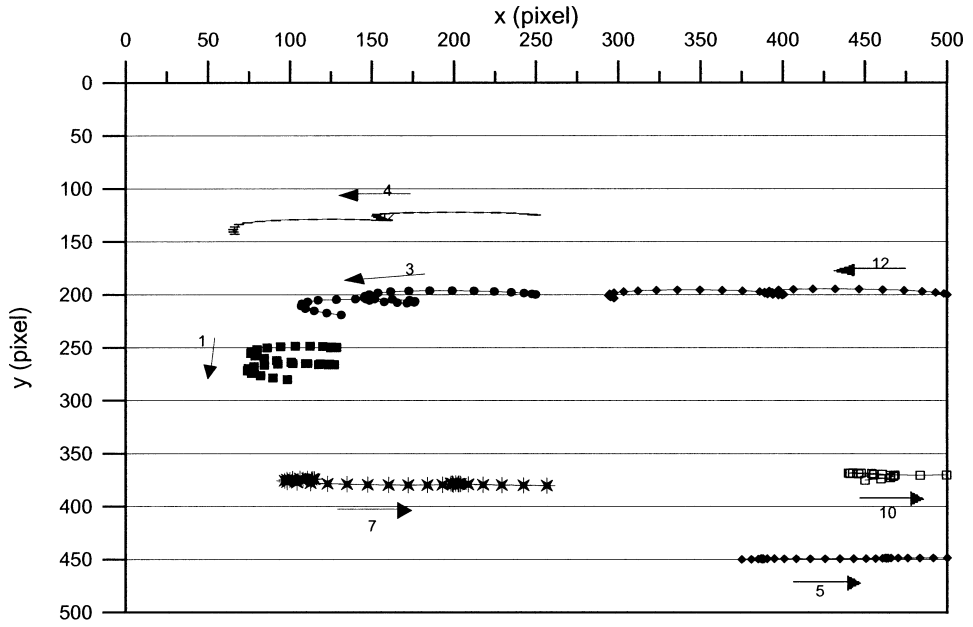


b)

**Fig. 3 Tracers trajectories observed in the *x–y* plane during 1000 s: a) experimental results (Foton 12) and b) numerical results.**

vector in fact well correlates the motion of the bubbles observed during the experiment.

Moreover, the tracers trajectories, detected with the charge-coupled device (CCD) camera, show the presence of a large convective cell with some helicoidal trajectories in the central part of the optical window (Figure 3a). The objective of the numerical study was the demonstration that the tracers motion was induced by the pendular oscillation of the cell. To explain and correlate the experimental results with the measured accelerations, three-dimensional numerical simulations have been performed, with the model presented earlier at the experimental conditions. The measured accelerations at the payload location are assigned as inputs to the numerical program. A linear dependence on the temperature $T$ ($1208.4–0.5298 \cdot T$ kg/m$^3$) has been considered for the density; a value of 0.66 W m$^{-1}$K$^{-1}$ has been considered for the thermal conductivity; the viscosity is a quadratic function of the temperature ($0.7397 - 0.004099 \cdot T + 5.7954e\text{-}6 \cdot T^2$ kg m$^{-1}$s$^{-1}$). The temperatures of the cold and hot walls are 30 and 80°C, respectively.

The maximum computed velocities are of the order of 6–7 $\mu$m/s. They are in agreement with the experimental velocities measured by the CCD camera. The field of view of the CCD was $2 \times 2$ cm (Fig. 3). Figure 3a shows some experimental trajectories detected during an observation time of 1000 s. Particle 4 and particle 5 in Fig. 3a move, respectively, from right to left and vice versa, which confirms the presence of a large counterclockwise circulation cell. The displacements of these particles are of about 150 pixels, corresponding to about 6.3 mm, that is, to an average velocity of 6.3 $\mu$m/s.

The helicoidal trajectories in the central portion of the optical window can be explained by the three-dimensional and time-dependent motions induced by the pendular accelerations on the cell. The three-dimensional trajectories resulting from the combined effect of the

buoyancy flow (mainly in the $x$–$y$ plane) and of this pendular motion (mainly in the $x$–$z$ plane) have been projected onto the $x$–$y$ plane to compare the numerical results with the experimental trajectories shown in Fig. 3a. A number of numerical tracers have been considered, approximately at the same initial positions of the tracers during the experiment. The computed trajectories in a time period of 1000 s are shown in Fig. 3b. The comparison with the experimental results is excellent.

## Typical Experiments on the ISS

### Thermal Diffusion in a Homogeneous Liquid

Numerical simulations have been carried out to assess the influence of the acceleration disturbances onboard the ISS for typical fluid dynamic experiments. A first case study deals with a fluid cell filled with a homogeneous liquid in presence of an imposed temperature difference (Fig. 4, where the lower and the upper walls that are shown are maintained at a temperature of 15 and 16°C, respectively). Because the temperature differences inside the cell are relatively small, the density of the system can be considered almost constant, and the thermofluiddynamic distortions are mainly induced by pendular accelerations. The section of the cell is $8 \times 8$ cm. The liquid is a silicone oil with kinematic viscosity of 0.65 cS.

To study the difference between linear and pendular accelerations two different situations are considered: 1) The fluid cell exhibits linear vibrations with acceleration amplitude $10^{-4} g_0$ and frequency 0.1 Hz and 2) the cell exhibits pendular accelerations with the same frequency (0.1 Hz) and the same acceleration amplitude ($10^{-4} g_0$ at the cell center of mass) around a point located at different distances (4 and 20 cm). This corresponds to different angular accelerations ($2.54 \times 10^{-2}$ rad/s$^2$ for a distance of 4 cm and $4.74 \times 10^{-2}$ rad/s$^2$ for a distance of 20 cm).

The selected magnitude and frequency of the acceleration correspond to the worst conditions according to the first measurements carried out onboard the ISS.[14,15] Figure 4 shows the temperature contours and the average velocity vectors in the fluid cell subjected only to pendular accelerations. The temperature difference between the upper wall and the lower one is 1 K, whereas the other two walls are adiabatic. The distance between the center of the cell and the center of rotation is 4 cm. The maximum computed average velocities are of the order of $7.5 \times 10^{-5}$ m/s; the convective field induces a distortion of the temperature field. In particular, eight convective cells are present, according to the flow pattern found by Gershuni (see Ref. 19) in a similar configuration.

If the distance between the cell and the center of rotation increases (Fig. 5), the convective disturbances in the cell decrease (average velocity of the order of $3.3 \times 10^{-6}$ m/s). This is explained by the fact that increasing the distance the angular displacement decreases ($\alpha = 0.0621$ rad for $d = 4$ cm and $\alpha = 0.012$ rad for $d = 20$ cm). Figure 6 shows the numerical results obtained in the case of linear vibrations orthogonal to the temperature gradient. In this case, the convective disturbances in the cell are negligible (average velocity of the order of $7 \times 10^{-8}$ m/s) and the temperature field is almost purely diffusive (Table 1). Consider the order of magnitude of two driving terms in Eq. (3) for the two cases (linear and pendular accelerations). In case of pendular accelerations around the center of the cell (which is very close to the case of Fig. 3) the driving term is $\rho \nabla \times \boldsymbol{g} \propto \rho \dot{\Omega}$. In presence of linear oscillations (Fig. 5), the driving term is $\nabla \rho \times \boldsymbol{g} \propto \rho \beta_T \Delta T \dot{\Omega}$. For the conditions investigated in Figs. 4 and 6, the ratio of these two terms is of the order of magnitude of $\beta_T \Delta T = 10^{-3}$. The numerical results show in fact that the maximum computed average velocity is $7 \times 10^{-8}$ in Fig. 6 and $7.5 \times 10^{-5}$ in Fig. 4, that is, the ratio of the average velocities is of the same order of the ratio of the driving forces.

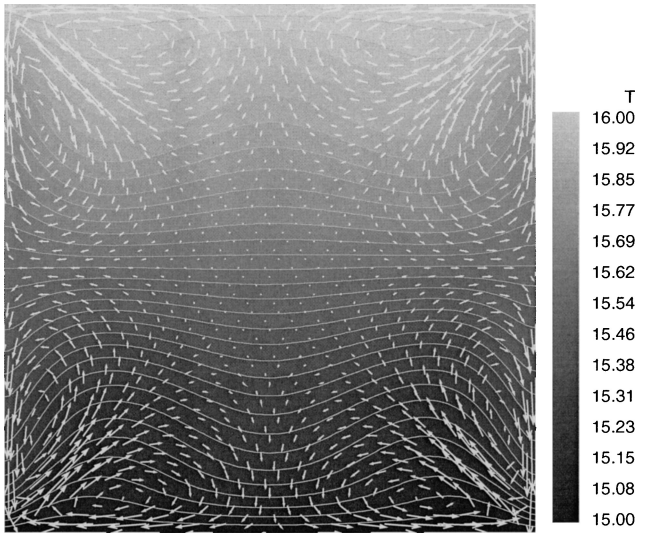


**Fig. 4 Temperature field and time average velocity in the case of pendular acceleration in a fluid cell filled with silicon oil 0.65 cS: $f = 0.1$ Hz, $b = 2$ cm, $\Delta T = 1$ K, and $v_{max} = 7.5e - 5$ m/s.**

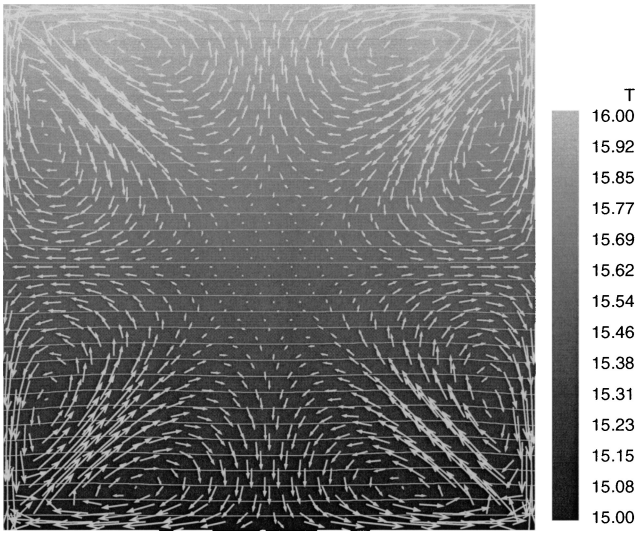


**Fig. 5 Temperature field and time average velocity in the case of pendular acceleration in a fluid cell filled with silicon oil 0.65 cS: $f = 0.1$ Hz, $b = 20$ cm, $\Delta T = 1$ K), and $v_{max} = 3.3e - 6$ m/s.**

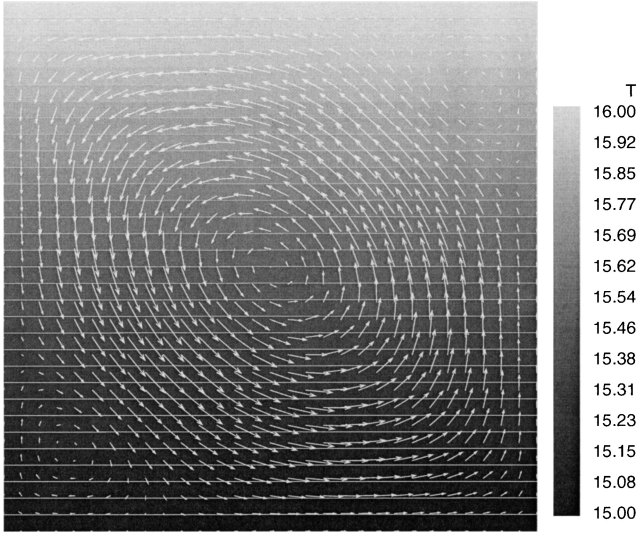


**Fig. 6 Temperature field and time-average velocity in the case of linear acceleration in a fluid cell filled with silicon oil 0.65 cS: $f = 0.1$ Hz, 0.0001 $g_0$, $\Delta T = 1$ K, and $v_{max} = 7e - 8$ m/s.**

### Species Diffusion and Solidification Experiments of Liquid Metals

In the environment of the ISS, vibrations at the payload location, for example, those induced by crew exercise, can affect sensitive

**Table 1 Summary of the numerical results in the case of a fluid cell with an imposed temperature difference[a]**

| $\Delta T$, K | Acceleration type | $v_{max}$ ($10^{-5}$ m/s) | Flow pattern |
|---|---|---|---|
| 1 | Pendular $f=0.1$ Hz, $r=4$ cm | 7.5 | 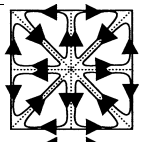 |
| 1 | Pendular $f=0.1$ Hz, $r=20$ cm | $3.3\times10^{-1}$ |  |
| 1 | Linear $f=0.1$ Hz, $g=0.001$ m/s$^2$ | $7\times10^{-3}$ | Almost purely diffusive |

[a]See Figs. 6–8.

science experiments. The active rack isolation system (ARIS)[20] has been developed to reduce, at rack level, the accelerations in a large range of frequencies above 0.1 Hz.

The isolation performances depend on the distance between the payload and the rack center of gravity so that, to minimize the acceleration level at the payload location, it is better to have the microgravity experiment near the rack c.g.[20] However, reduction of the linear acceleration does not imply reduction of the angular accelerations induced in the ARIS racks by the presence of umbilicals. In fact, different attenuator factors at different points of the rack imply pendular oscillations around the rack c.g.

Numerical simulations have been carried out under the assumption that the experiment payload is at the c.g. of the standard rack hosting the facility, for two different conditions: first, the rack is hardmounted, that is, the payload is subject to a linear acceleration of 0.01 $g_0$ at frequency $f=2$ Hz. The amplitude and frequency of the acceleration have been selected according to the theoretical predictions provided by NASA for the ISS complete assembly[20]; second, the rack is isolated by the ARIS, so that the linear acceleration at the rack c.g. is zero, but a pendular oscillation is present around the c.g. because the acceleration is not reduced at the top of the rack. When a distance of about 20 cm is considered, the acceleration of 0.01 $g_0$ results in an angular displacement of about 0.18 deg at the same frequency ($f=2$ Hz).

The first examined problems deals with the isothermal diffusion of a binary liquid mixture in a cavity with high aspect ratio ($10\times2.5$ cm$^2$). The liquid properties are typical of liquid metals: $\nu=10^{-3}$ cm$^2$/s and $D=10^{-5}$ cm$^2$/s. The initial concentration distribution is as follows: The cell is partitioned in two regions of the same size, and two different concentrations are prescribed in each region. At time $t=0$ the diffusion process starts. The condition $\partial c/\partial n=0$ is imposed at the walls, where $n$ is the normal to the wall. The density difference induced by the concentration difference is very small $\beta_c\Delta c=0.001$, where $\beta_c$ is the solutal expansion coefficient and $\Delta c$ the initial concentration difference) so that the process is quasi isodense.

Figure 7 shows the numerical results after $t=3$ h. In particular Fig. 7a shows the concentration field in the case of linear acceleration; the velocities are almost zero and the species distribution is almost coincident with the purely diffusive situation. Figure 7b shows the concentration distortions induced by the convective disturbances in the case of pendular accelerations.

Figure 8 shows the numerical results corresponding to $t=14$ h. The case of linear acceleration is shown in Fig. 8a. The flow pattern in Fig. 8b consists of eight convective cells located at the corners of the cavity. The convective motion induced by the pendular acceleration gives rise to a more uniform concentration field; the difference of the concentrations at the two sides of the cell is still about 1 in the cases of linear $g$-jitter (Figs. 7a and 8a), whereas it is 0.53 after 3 h (Fig. 7b) and 0.023 after 14 h (Fig. 8b) in presence of convective motions due to pendular oscillations.

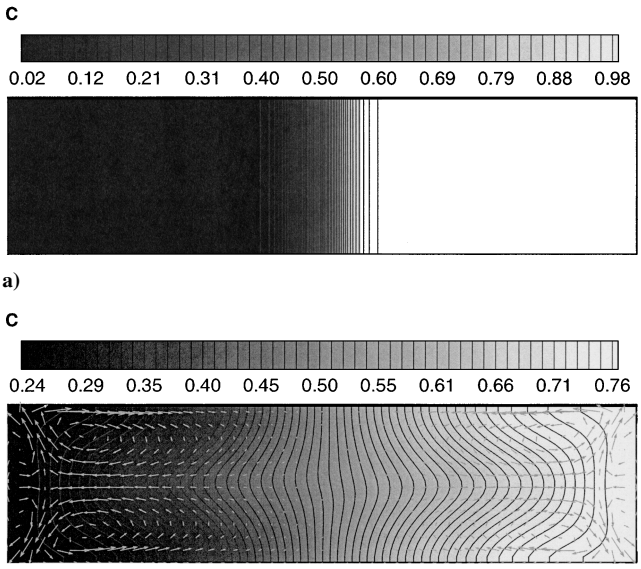


**Fig. 7 Isothermal diffusion experiment; concentration field and velocity vectors after $t=3$ h, cell oscillating around a point located at $r=20$ cm: a) linear accelerations and b) pendular accelerations, $v_{max}=5.0\times10^{-5}$ m/s.**

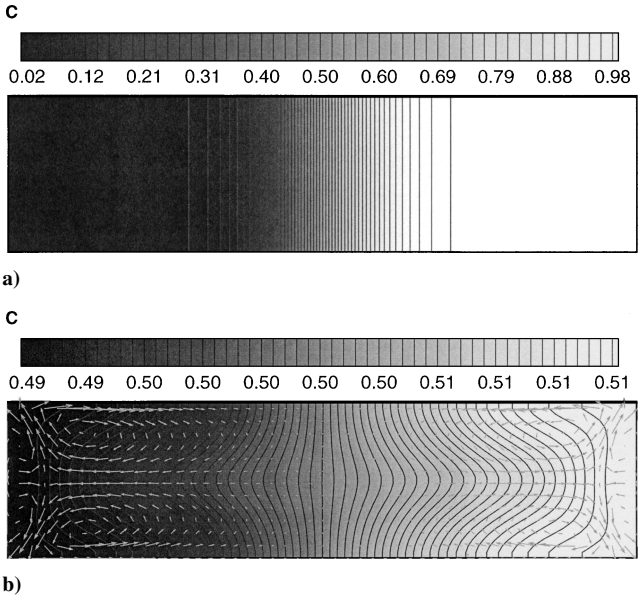


**Fig. 8 Isothermal diffusion experiment; concentration field and velocity vectors after $t=14$ h, cell oscillating around a point located at $r=20$ cm: a) linear accelerations and b) pendular accelerations $v_{max}=5\times10^{-5}$ m/s.**

An additional problem of interest for the future ISS experimentation is a typical solidification experiment with the horizontal Bridgman technique. The liquid properties are the same as in the preceding case. A temperature gradient is established in the horizontal direction (100 K/cm).

The thermal expansion coefficient is $2\times10^{-4}$ K$^{-1}$, and the thermal diffusivity is $10^{-1}$ cm$^2$/s. The boundary conditions for the concentration, resulting from the model described in Ref. 21, are

$$\frac{\partial c}{\partial x}=Pe\frac{1-k}{k}e^{-Pe}, \qquad \text{at } x=0 \tag{20}$$

$$\frac{\partial c}{\partial x}=Pe\frac{1-k}{k}, \qquad \text{at } x=L \tag{21}$$

$$\frac{\partial c}{\partial y}=0, \qquad \text{on the upper and lower walls} \tag{22}$$

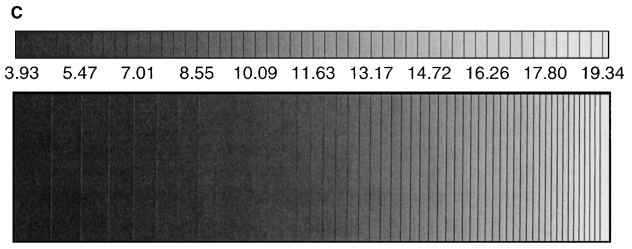


**Fig. 9 Initial concentration field for the solidification experiment.**

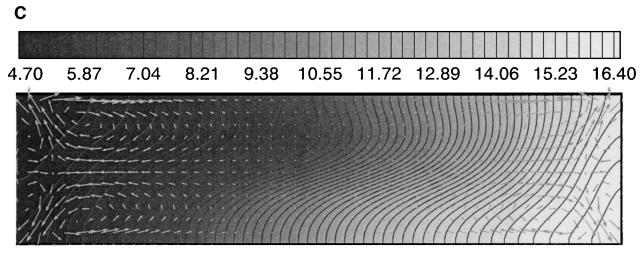


a)

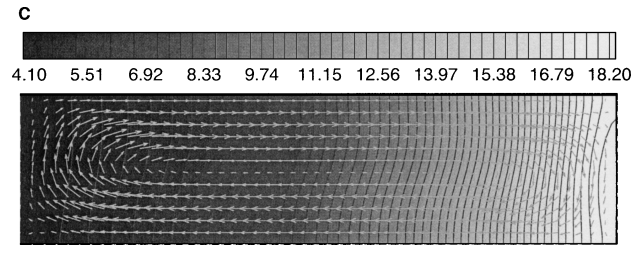


b)

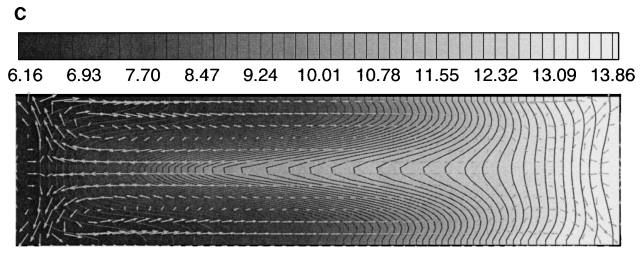


c)

**Fig. 10 Solidification experiment; concentration field and velocity vectors after $t = 3$ h, cell oscillating around a point located at $r = 20$ cm: a) linear accelerations $v_{max} = 1.38 \times 10^{-6}$ m/s, b) linear accelerations $v_{max} = 1.38 \times 10^{-8}$ m/s, and c) pendular accelerations $v_{max} = 2.88 \times 10^{-5}$ m/s.**

where $k$ is the segregation coefficient, $Pe = VL/D$, $V$ is the growth velocity (order of magnitude of $10^{-6}$ m/s), $D$ is the diffusion coefficient ($10^{-5}$ cm$^2$/s), and $L$ the reference length. In this specific case, we considered a value of $Pe = 2$ and $k = 0.05$. The initial temperature and concentration distributions correspond to the purely diffusive situation. In particular, the temperature exhibits a linear distribution along the cavity; the concentration distribution (shown in Fig. 9) is taken according to the model discussed in Ref. 21.

When a linear periodic acceleration (with the same amplitude and frequency of the preceding case) is applied in the vertical direction (orthogonal to the temperature gradient), the average flow pattern consists of convective cells located close to the cell corners (Fig. 10a). If the amplitude of the linear acceleration is reduced by one order of magnitude (0.001 $g_0$), a single clockwise convective cell, appears in the cell, but the velocities are reduced by two orders of magnitude (Fig. 10b). The convective disturbances give rise to distortions of the concentration distribution that are obviously smaller when the acceleration amplitude is reduced by one order of magnitude.

Figure 10c shows the situation in the case of pendular acceleration (corresponding to the same amplitude and frequency of Fig. 10a, and a distance of 20 cm from the rotation center). In this configuration, the average velocity is larger than in the linear case, and larger distortions of the concentration field are evident.

## Ground Experiments and Numerical Correlation

To study the streaming flow induced by high-frequency pendular accelerations, the same experimental configuration of the Foton was investigated on the ground. A cell ($5 \times 5 \times 2$ cm$^3$) was filled with a solution of 50% ethylene glycol in water. The main difference with the Foton consists in that, to analyze the streaming flow, high-frequency pendular oscillations ($f = 5$ and 10 Hz) have been investigated.

Figure 11 shows a schematic view of the experimental facility, including a rotating platform, an electric motor that provides the pendular motion, and an accelerometer that measures the tangential acceleration (and, consequently, the sinusoidal angular displacement). The system includes a plexiglass support for the laser diode and a CCD video camera. Tracers with the same density as the liquid solutions are used to visualize the motion in a plane illuminated by the laser sheet. Two micrometric position stages allow the change of the relative position between the experimental cell and the axis of the rotating platform. The CCD camera can be translated vertically to change the field of view.

A parametric analysis has been carried out to study the convective disturbances at different frequencies and different angular displacements. Three experimental tests are reported, corresponding to a pendular motion with a frequency $f = 5$ Hz at two values of

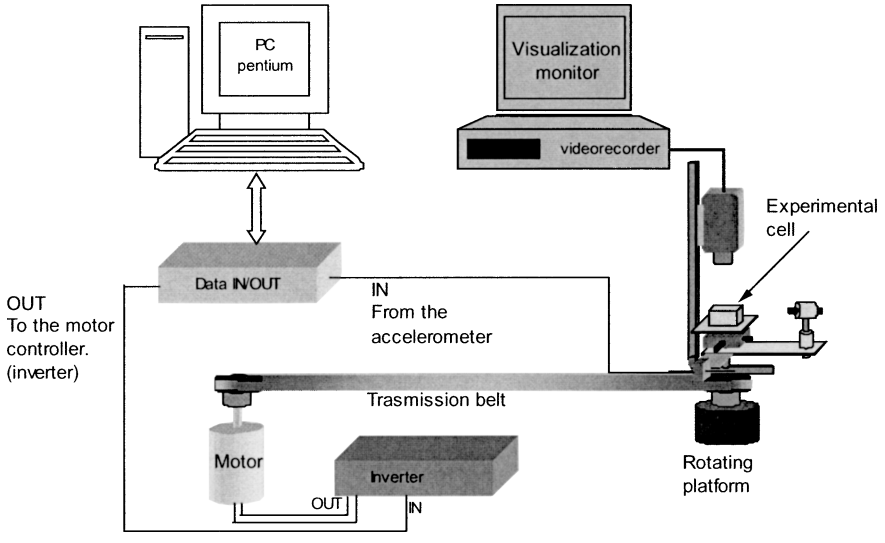


**Fig. 11 Schematic of experimental apparatus.**

**Table 2 Comparison between computed and measured accelerations for the same case as Fig. 15**

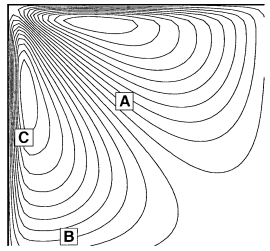


Schematic view of the stream line and positions where the experimental velocity have been measured.

| Frequency, Hz | $\alpha_{0K}$, rad | Experimental ($10^{-2}$ cm/s) | | | Numerical ($10^{-2}$ cm/s) | | |
|---|---|---|---|---|---|---|---|
| | | A | B | C | A | B | C |
| 5 | 0.04 | 1.6 | 0.55 | 2.2 | 2.0 | 0.32 | 2.96 |
| 5 | 0.067 | 4.8 | 1.34 | 5.6 | 4.9 | 0.89 | 6 |
| 10 | 0.04 | 3.5 | 1.0 | 6.0 | 4.2 | 0.7 | 6.6 |

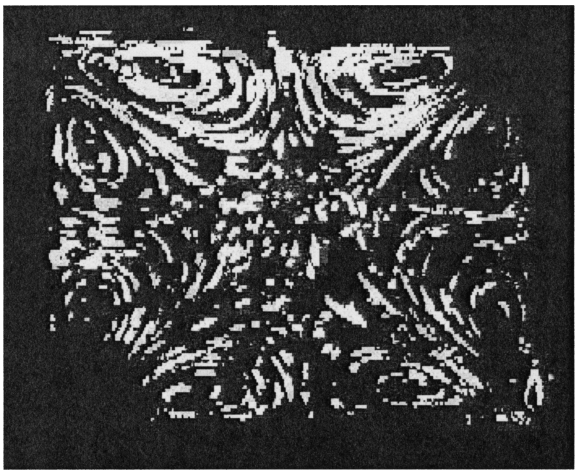

a)

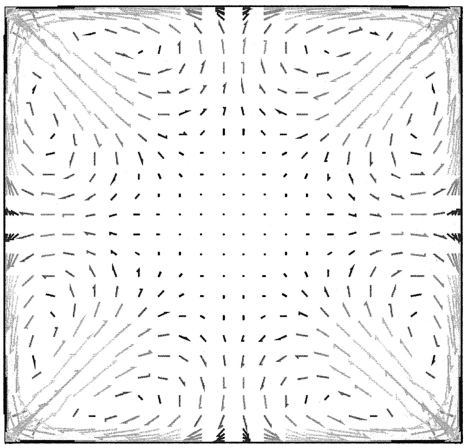

b)

**Fig. 12 Fluid cell filled with a mixture of ethylene glycol and water (50%) subject to pendular acceleration, $f = 10$ Hz and $\alpha = 0.04$ rad: a) path lines of the experiment and b) computed velocity vectors.**

$\alpha$ ($\alpha = 0.04$ rad, $\alpha = 0.067$ rad) and at $f = 10$ Hz ($\alpha = 0.04$ rad). Figure 12a shows the typical average flow pattern observed in the cell. The stream lines show eight symmetrical vortex cells. The fluid moves along the cavity walls from their center toward the corners, thus, forming plane jets along the diagonals passing from the square corners to its center.

Two-dimensional numerical computations have been performed at the same conditions as the experimental tests. The corresponding computed average velocity field is shown in Fig. 12b. Table 2 shows a comparison between the experimental and the numerical results. In particular, the average velocities have been taken at the locations A, B, and C indicated at the top of Table 2. According to Gershuni and Lyubimov,[19] the average velocities induced by high-frequency pendular motions, in isothermal conditions, are $V \propto \alpha^2 f L$. The results in Table 2 confirm this theoretical prediction. Table 2 shows sufficient correlation between numerical and experimental velocity, especially at location A; this is because velocity is almost constant in a wide part of the diagonal of the convective cell and this allows a quantitative comparison between the numerical and the experimental results. On the contrary, the large velocity gradients make it difficult to establish quantitative numerical–experimental correlations in locations B and C (Table 2). In particular, the measured velocities along C are always smaller than the numerical ones. In recognition that there are large variations of the velocities moving from the center of the convective cell to the wall, the agreement between the numerical and the experimental results can be considered satisfactory.

## Conclusions

The influence of residual acceleration on fluid physics experiments in a microgravity environment has been analyzed considering quasi-steady, linear and pendular time-dependent accelerations.

The different driving forces in the vorticity equation have been considered to investigate the contributions leading to convective motion in a fluid cell. Steady and linear time-dependent accelerations generate convection in an otherwise quiescent fluid only in the presence of density gradients. Pendular acceleration may induce convective motion even in the absence of density gradient induced by temperature and/or species concentration differences.

The numerical simulations, carried out for different study cases, have shown that pendular acceleration may induce convective disturbances even in quasi-isodense processes (negligible temperature and/or species concentration gradients). Therefore, the three components of the linear acceleration at the experimental cell location are not sufficient to correlate the thermofluid-dynamic field with the microgravity environment, but the knowledge of the angular accelerations is very important. A good correlation was found between numerical and experimental results obtained in microgravity and ground laboratories.

## Acknowledgments

This work has been partially supported by the ESA and by the Italian Space Agency.

## References

[1]Alexander, J. I. D., "Low Gravity Experiment Sensitivity to Residual Acceleration: A Review," *Microgravity Science and Technology*, Vol. 3, No. 2, 1990, pp. 52–68.

[2]Arnold, W., Iacqmin, D., Gaug, R., and Chait, A., "Three-Dimensional Flow Transport Modes in Directional Solidification During Space Processing," *Journal of Spacecraft and Rockets*, Vol. 28, No. 2, 1991, pp. 238–243.

[3]Chen, W. Y., and Chen, C. F., "Effect of Gravity Modulation on the Stability of Convection in a Vertical Slot," *Journal of Fluid Mechanics*, Vol. 395, 1999, pp. 327–344.

[4]Farooq, A., and Homsy, G. M., "Linear and Non-Linear Dynamics of a Differentially Heated Slot Under Gravity Modulation," *Journal of Fluid Mechanics*, Vol. 313, 1996, pp. 1–38.

[5]Garandet, J. P., Corre, S., and Favier, J. J., "Acceptable Microgravity Levels in Bridgman Solidification-Scaling Analysis and Experiments," *Microgravity Science and Technology*, Vol. 11, No. 2, 1998, pp. 59–62.

[6]Monti, R., Langbein, D., and Favier, J. J., "Influence of Residual Accelerations on Fluid Physics and Material Science Experiments," *Fluid and Material Science in Space*, edited by H. U. Walter, Vol. 3, Springer-Verlag, Berlin, 1987, p. 52.

[7]Monti, R., and Savino, R., "Microgravity Experiment Acceleration Tolerability on Space Orbiting Laboratories," *Journal of Spacecraft and Rockets*, Vol. 33, No. 5, 1996, pp. 707–716.

[8]Monti, R., Savino, R., Alterio, G., and Fortezza, R., "Experimental and Numerical Study of Thermovibrational Convection," *Journal of Thermophisics and Heat Transfer*, Vol. 13, No. 1, 1998, pp. 161–163

[9]Monti, R., and Savino, R., "G-Sensitivity of Microgravity Experimentation: Fundamentals of Disturbance Response," *International Journal for Microgravity Science and Technology*, Vol. 12, No. 2, 1999, pp. 1–6.

[10]Savino, R., and Monti, R., "Fluid-Dynamic Experiment Sensitivity to Accelerations Prevailing on Microgravity Platforms," *Physics of Fluids in Microgravity*, Gordon and Breach, New York, 2001, pp. 515–559.

[11]"ISS DAC-6 Integrated Loads and Dynamic Analytical Model Properties," The Boeing Company, Rept. A92-J195-STN-M-WLP-980050, Houston, TX, April 1998.

[12]"Integrated Loads and Dynamics Verification Plan," The Boeing Company, Rept. D684-10288-01, ISS International Space Station Program, Houston, TX, Aug. 1999.

[13]Kazakova, A. E., "The Result on Flight Experiment on Determination of Microaccelerations Level on 'Foton 11' Spacecraft," 50th International Astronautical Federation Congress, Paper IAF-99-J.3.06, Oct. 1999.

[14]Jules, K., Hrovat, K., Kelly, E., McPherson, K., and Reckart, T., "International Space Station Increment-2 Microgravity Environment Summary Report," NASA TM-2002-211335, April 2002.

[15]Jules, K., McPherson, K., Hrovat, K., and Kelly, E., "Initial Characterization of the Microgravity Environment of the International Space Station," 53rd International Astronautical Congress, Paper IAC-02-J.6/T.5.02, Oct. 2002.

[16]DeLombard, R., Hrovat, K., Kelly, E., McPherson, K., and Jules, K., "An Overview of the Microgravity Environment of the International Space Station Under Construction," AIAA Paper 2002-0608, Jan. 2002.

[17]Patankar, S. V., *Numerical Heat Transfer and Fluid Flow*, Hemisphere, Washington, DC, 1980, pp. 1–197.

[18]Albanese, C., Peluso, F., and Castagnolo, D., "Thermal Radiation Forces in Microgravity; The True and Tramp experiments. Results and Future Perspectives," *First International Symposium on Microgravity Research and Applications in Physical Sciences and Biotechnology*, SP 454, ESA, 2001, pp. 755–768.

[19]Gershuni, G. Z., and Lyubimov, D. V., *Thermal Vibrational Convection*, Wiley, New York, 1998, pp. 344–350.

[20]Bushnell, G., and Fiahlo, I., "Active Rack Isolation System. Program and Technical Status," *19th International Microgravity Measurement Group Meeting*, NASA CP-2000-210374, Oct. 2000.

[21]Alexander, J. I. D., "Response of Crystal Growth Experiment to Time Dependent Residual Acceleration," *Lecture Notes on Physics*, edited by L. Ratke, H. Walter, and B. Feuerbacher, No. 464, Springer, Berlin, 1995, pp. 95–104.

A. Ketsdever
*Associate Editor*